tions inferred from the "split" amorphous band and the mode of crystallization seems to be consistent with this picture. Although this simple model can account for easy glass-forming systems, its role in the present case should be viewed with caution because of the tremendous crystallization tendency of aluminum. Thus, the unusual formability of these glassy aluminum alloys deserves further studies.

High tensile strengths are expected, in general, for metallic glasses. Tensile fracture strengths of aluminum-based metallic glass ribbons are listed in Table 1. These strengths, in general, greatly exceed the strongest commercial aluminum alloys. For an aluminum alloy to achieve a strength of greater than 500 MPa, it must be highly developed and carefully thermally treated to peak strength. At a strength of 940 MPa the $Al_{90}Fe_5Ce_5$ alloy is the strongest we tested. The $Al_{87}Fe_{8.7}Gd_{4.3}$ and $Al_{87}Ni_{8.7}Y_{4.3}$ alloys have strengths near the Al-Fe-Ce material and, with modification of the ratio of elements, these values could undoubtedly be improved upon. When examined in SEM the fracture surfaces are fairly typical of metallic glass material. A typical fracture surface is shown in Fig. 4. This micrograph is of the $Al_{90}Fe_5Ce_5$ alloy and although not much ductility is observed (that is, no overall necking) the material does not fracture in a completely brittle fashion. The vein structure consists of protrusions on the fracture surfaces. These markings can be taken as evidence of local necking (*10*). We can describe the fracture of metallic glasses as "ductile" if it is a result of, at least locally, large plastic strains. In uniaxial tension, it occurs along the plane of the shear band. In tension, at relatively high stresses, metallic glasses deform extremely inhomogeneously. A large number of shear bands are visible within 20 μm below the fracture surface. Further examination of the ribbon failed to reveal any slip activity in areas other than near the fracture surface. Young's modulus data listed in Table 1 were determined from the elastic portion of the force versus displacement curve. Thirty-millimeter gauge sections were used and tested in a similar fashion as the tensile fracture tests. Several tests were run for each specimen. In general the material with the highest fracture strengths also showed the higher Young's modulus data. The modulus of the $Al_{90}Fe_5Ce_5$ metallic glass was the highest at 66 GPa. It is expected that the present class of alloys will receive much attention as potential high-strength, low-density materials. Although the current alloys discussed in this report have moduli lower than crystalline aluminum alloys, it is suggested that with further research the properties can be optimized.

REFERENCES AND NOTES

1. S. Samson, *Acta Crystallogr.* **11**, 851 (1958).
2. After our work was completed, we learned of an independent report of glassy phases in Al-Y-Ni, Al-Ni-Zr, Al-Hf-Ni, Al-Y-M, and Al-La-M (M = Fe, Co, Ni, Cu) alloys by A. Inoue, K. Ohtera, A. P. Tsai, T. Masumoto, *Jpn. J. Appl. Phys.* **27**, L479 (1988).
3. T. Egami and Y. Waseda, *J. Non-Cryst. Solids* **64**, 113 (1984).
4. F. Spaepen and D. Turnbull, *Annu. Rev. Phys. Chem.* **35**, 241 (1984).
5. H. A. Davies, in *Amorphous Metallic Alloys*, F. E. Luborsky, Ed. (Butterworths, Boston, 1983), pp. 8–25.
6. D. M. Follstaedt and S. T. Picraux, in *Alloy Phase Diagrams*, L. H. Bennett, B. C. Giessen, T. B. Massalski, Eds. (Materials Research Society, Pittsburgh, 1984), pp. 94–101; also J. A. Knapp and D. M. Follstaedt, *Phys. Rev. Lett.* **56**, 1827 (1986).
7. A. Inoue, A. Kitamura, T. Masumoto, *J. Mater. Sci.* **16**, 1895 (1981); R. O. Suzuki, Y. Komatsu, K. E. Kobayashi, P. H. Shingu, *ibid.* **18**, 1195 (1983).
8. H. J. Leamy, H. S. Chen, T. T. Wang, *Metall. Trans.* **3**, 699 (1972).
9. P. H. Gaskell, in *Glassy Metals II*, H. Beck and H. J. Guntherodt, Eds. (Springer-Verlag, New York, 1983), pp. 5–49.
10. F. Spaepen and A. I. Taub, (*4*), pp. 231–256.

11. This work was supported by the U.S. Army Research Office Contract No. DA AL03-87K-0057.

19 July 1988; accepted 12 August 1988

Dynamic Instability of Sheared Microtubules Observed by Quasi-Elastic Light Scattering

ROBERT A. B. KEATES* AND F. ROSS HALLETT

The kinetics of microtubule reassembly was studied in vitro by quasi-elastic light scattering (QELS). When microtubules assembled in the absence of microtubule-associated proteins (MAPs) were sheared, they rapidly depolymerized, recovered, and reassembled. The mean length of the recovered microtubules was the same as that observed just before shearing, implying that on average one fragment per original microtubule survived the fragmentation and recovery. When microtubules that contained 25 percent brain MAP were sheared, the fragments did not depolymerize extensively and the average length of the fragments decreased by a factor of 3 relative to the unsheared sample. The results support the dynamic instability model, which predicts that cellular microtubules are latently unstable structures protected on their ends by stabilizing caps.

THE DYNAMIC INSTABILITY HYPOTHESIS of microtubule assembly proposed by Mitchison and Kirschner (*1*) provides a ready explanation for many aspects of cell morphogenesis (*2*). We have adapted QELS to observe the dynamic instability of microtubules reassembled in vitro. The diffusive motions of microtubules in solution can be measured by QELS, from which the length distribution of a population can be calculated (*3, 4*). We observed clear evidence for dynamic instability in populations of microtubules, from their depolymerization and regrowth after shearing, in samples of microtubules assembled from purified tubulin, free of MAPs. The disassembly of the microtubules after shearing was consistent with the presence of protective caps at the ends of latently unstable polymers (*5, 6*). For microtubules that contained MAPs, we observed little depolymerization and regrowth of microtubules after shearing: the lack of depolymerization implied that MAP-containing microtubules were stable through most of their length.

Microtubules that are dynamically unstable should exist in two phases, one unstable and one stable. Rapid disassembly of the unstable population releases subunits that can contribute to the continued growth of

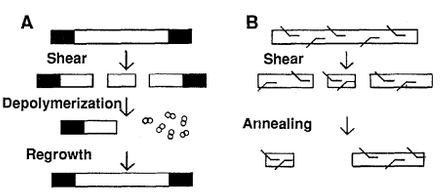

Fig. 1. Schematic outline of the experiments. In (**A**), MAP-free microtubules are shown terminated with protective caps that mask an unstable core. In the GTP-cap hypothesis, the caps contain tubulin-GTP, whereas the core is tubulin-GDP (*5*). When microtubules are fractured by shearing, uncapped fragments depolymerize rapidly, which releases tubulin subunits that can exchange GDP for GTP. The tubulin-GTP can then add to fragments that retain stable caps, allowing regrowth. In (**B**), MAPs bound to microtubules stabilize the polymer, so little depolymerization occurs on shearing and stable fragments are obtained. Over a period of time, some fragments may join and anneal, increasing the average length under steady-state conditions (*10*).

R. A. B. Keates, Biophysics Interdepartmental Group, Department of Chemistry and Biochemistry, University of Guelph, Guelph, Ontario, Canada N1G 2W1.
F. R. Hallett, Biophysics Interdepartmental Group, Department of Physics, University of Guelph, Guelph, Ontario, Canada N1G 2W1.

*To whom correspondence should be addressed.

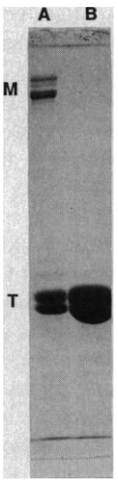

Fig. 2. SDS–polyacrylamide gel electrophoresis profiles of (**A**), 8 μg of microtubule protein containing MAPs and (**B**) 40 μg of MAP-free tubulin (M, MAPs; T, tubulin).

the stable population (*1*). Experimental observation of dynamic instability is based on measuring changes in microtubule length. A population of microtubules must be sampled at intervals and then fixed and stained to be measured by electron microscopy or immunofluorescence microscopy (*1, 7*). Fluctuations in the length of single microtubules have also been observed directly, by dark-field microscopy (*8*). Such labor-intensive measurement of individual microtubules has limited the sample sizes for both methods, in particular for direct observation in dark field.

With QELS, we can measure the collective properties of a large population (about 10^4 to 10^5 microtubules) noninvasively, subjected only to illumination by a low-power HeNe laser. Measurements on the same sample can be repeated at intervals of 100 to 600 s, depending on the extent of polymerization. The result of each measurement was a distribution of lengths from which we determined the number-average length.

Dynamic instability is thought to arise because of the marked difference in polymerization kinetics between tubulin that contains bound guanosine triphosphate (GTP) versus tubulin that contains bound guanosine diphosphate (GDP) (*1*). In the microtubule, hydrolysis of the bound GTP produces tubulin-GDP that can depolymerize 1000 times as fast as tubulin-GTP, resulting in catastrophic disassembly. However, subunit exchanges between polymer and monomer can only occur at the ends of microtubules (*7*). Thus a microtubule may contain mostly tubulin-GDP throughout its length, provided that the ends are protected by a stable cap of tubulin-GTP subunits (*5*). The latent instability of this organization can be revealed by shearing, which exposes the unstable tubulin-GDP (Fig. 1). Depolymerization releases tubulin as free subunits, which can exchange bound GDP for GTP, whereas tubulin within an intact microtubule is unable to exchange its bound nucleotide (*5*). The free tubulin-GTP can then reassemble by adding to a microtubule that has a stable cap.

Two identical samples of bovine brain MAP-free tubulin (*9*) were polymerized and monitored (Fig. 2), one in the spectrophotometer to measure the mass of polymerized tubulin and the second in the photon-correlation spectrometer for QELS and length determination (*10*). The experiments ran concurrently. Each sample was allowed to reach apparent steady state, as revealed by the plateau in the development of turbidity (Fig. 3A). At this point, the average length was 25 μm. The sample was then sheared. With the spectrophotometer, we were able to resume measurement within 3 to 5 s of shearing. As predicted by dynamic instability and the cap hypothesis, the shearing initiated massive depolymerization, to 75% of the steady-state level. The depolymerization process continued briefly while the turbidity was monitored (Fig. 3B). The fast response of the spectrophotometer (SLM-Aminco DW2C, Urbana, Illinois) precluded the superimposition of any electronic lag or damping on actual changes in the sample turbidity. The mass of polymer began to increase 30 s after shearing; the rate of increase was comparable to that of the original polymerization. The maximum recovery rate was observed at 0.04 absorbance unit and was faster than the original growth rate at 0.04 absorbance unit by a factor of 1.6. As the system approached steady state, the ratio of rates of recovery to growth tended to 1.0.

The QELS sample could not be monitored reliably for 5 min after shearing, because of residual turbulence in the solution. When measurements resumed, both the mass of polymer as measured spectrophotometrically and the length as measured by QELS returned to their original steady-state values. The final polymer length, 25 μm, was the same as the length just before shearing, which implies that the final number of microtubules was the same as before shearing. Because each original microtubule should have generated two fragments with caps, roughly one original cap survived the shear-induced disassembly and subsequent recovery. Because the recovery curves are similar to the original assembly progress curves in the later stages, the disappearance of sheared microtubule fragments appeared to occur mostly during the rapid disassembly phase. However, some reduction in microtubule number must occur in the recovery phase during approach to steady state, to account for the length increase after 3000 s. Evidence against a contribution from annealing is suggested by the abrupt termination of further growth at 3600 s; if annealing occurred, it should have continued indefinitely. Unsheared samples maintained a steady length for 5500 s and showed no signs of annealing under identical conditions. The system was pushed far from steady state by the synchronous shear-induced depolymerization, and less stable polymeric structures could initially participate in the regrowth, for example, semistable microtubule fragments growing at one end and depolymerizing at the other. On return to steady state, the free subunit pool would be depleted and only fully stable microtubules would survive. Our understanding of the non–steady-state dynamics is limited, and further experimental work will be necessary to account for these events. It is

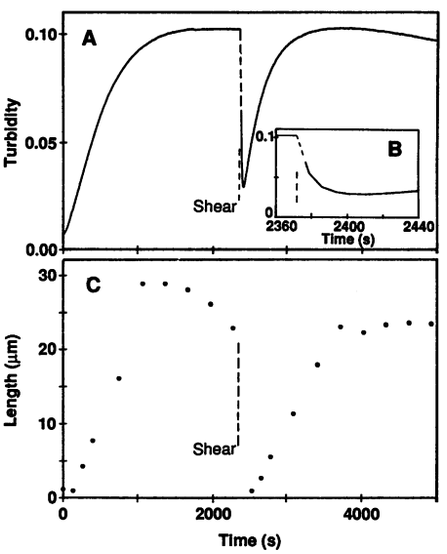

Fig. 3. Polymerization and shearing of MAP-free tubulin. (**A**) Turbidity profile (330 nm). Turbidity is proportional to the mass of polymerized tubulin. We incubated 10 μl of tubulin (1.2 mg/ml) in 3*M* glycerol, 0.1*M* Pipes K^+, 5 m*M* magnesium acetate, 1 m*M* EGTA, 1 m*M* GTP, *p*H 6.8, at 37°C in a cuvette. This tubulin would only nucleate new microtubules if glycerol was present but could elongate existing microtubules in the absence of glycerol. After 10 min to allow microtubule polymerization, 1.5 ml of tubulin (1.2 mg/ml) in 100 m*M* Pipes K^+, 1 m*M* magnesium acetate, 1 m*M* EGTA, 1 m*M* GTP, pyruvate kinase (1 μg/ml), 4 m*M* phosphoenolpyruvate, *p*H 6.8, was prewarmed to 37°C and added. This tubulin concentration assembled to 0.3 mg of microtubules per milliliter, based on a critical concentration of 0.9 mg/ml. At the point indicated by the vertical broken line, the sample was sheared by passage through a needle (26 gauge by 1 cm) with three strokes of the syringe. (**B**) The same turbidity profile on an expanded time scale for 60 s after shearing. (**C**) Plot of number-average microtubule lengths estimated by QELS (*10*). The data represented in Figs. 3 and 4 have been reproduced on three occasions with different preparations of protein.

clear, however, that after return to steady state, the number-average microtubule length is unchanged, and hence the number of microtubules is the same as before shearing.

In other shearing experiments, regrown microtubules could be sheared a second or third time with the same results. The extent of depolymerization and the progress of recovery were similar whether shearing was mild or more vigorous, suggesting that the survival of fragments for regrowth was not dependent on the number of fragments generated. Manipulation as mild as a single inversion of the sample cuvette could trigger partial depolymerization.

Bovine brain microtubule protein containing 25% MAPs and 74% tubulin was examined in a second series of experiments (Fig. 4). When the polymer mass reached apparent steady state, the sample was sheared. A minor discontinuity in the turbidity profile represented less than 10% depolymerization. Turbidity was always increasing by the time measurement resumed (3 to 5 s after shearing). Turbidity recovered very rapidly, consistent with a large number of growing microtubule ends, which indicated that most fragments participated in the regrowth process. The average microtubule length measured by QELS was reduced from 16 to 5 μm after shearing. Over a period of 40 min, the average length increased to 6 μm. However, the increase in length was not synchronized with the increase in turbidity, so this polymerization did not involve tubulin subunits released by the shearing process and occurred while the microtubules were at apparent steady state. The size of MAP-rich microtubule fragments after shearing was dependent on the extent of shearing.

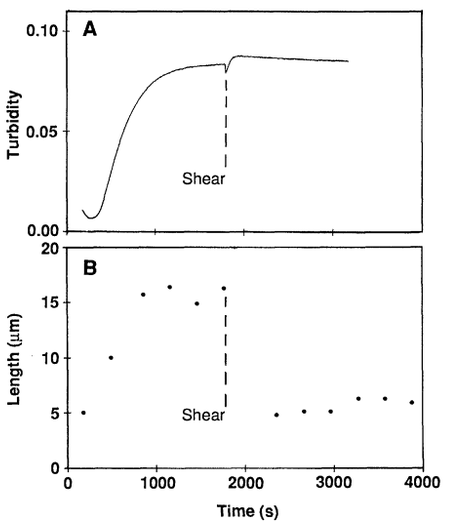

Fig. 4. Polymerization and shearing of microtubule protein that contained 25% MAPs. (**A**) Turbidity profile (330 nm). Microtubule protein (1.5 ml or 0.64 mg/ml) was incubated at 37°C in 0.1*M* Pipes K^+, 1 m*M* magnesium acetate, 1 m*M* EGTA, 1 m*M* GTP, pyruvate kinase (1 μg/ml), 4 m*M* phosphoenolpyruvate, *p*H 6.8. Under these conditions, spontaneous nucleation of microtubules occurred. The concentration of microtubule protein used gave 0.4 mg of microtubules per milliliter, including MAPs, based on a critical concentration of 0.24 mg/ml in this buffer. Shearing was as described in Fig. 3. (**B**) Plot of number-average microtubule lengths estimated by QELS.

The observation that MAP-free microtubules continued to depolymerize after shearing confirms the prediction of the dynamic instability hypothesis that a stable cap may protect a latently unstable microtubule core (*1*). The exact nature of this stable cap remains to be identified, but the GTP cap model (*5*) remains most consistent with our observations on the purified tubulin used in these experiments. We have consistently found that, after shearing, MAP-free microtubules regrow to lengths similar to the original unsheared population. Thus few sheared fragments were able to recover and regrow. The conditions of incubation would not have allowed spontaneous nucleation of new microtubules from the free tubulin released. We cannot tell whether the regrown microtubules resulted from random recovery of fragments or from the survival of one or other of the original caps. The apparent lack of dependence on the extent of shearing suggests the latter but needs further study. In this context, Walker *et al.* have reported that the frequency of rescue at the minus, or kinetically slow, end of the microtubules was an order of magnitude greater than at the plus, or kinetically fast, end (*11*). Fragments not rescued would depolymerize to their subunits.

The large changes in turbidity indicate that release and reincorporation of subunits occurred during the first 600 s after shearing, but length continued to increase for an additional 600 s (Fig. 3A). Microtubules may also increase their average length by joining end to end and annealing (*12*). Under our experimental conditions, undisturbed microtubules did not increase their average length at steady state. Thus we do not believe that annealing makes a significant contribution at the low microtubule concentration (10^{-10}*M*) in our experiments. We argue that the continued increase in length results from the dynamics induced by shearing. Immediately after shearing, the free tubulin concentration increases and a subpopulation may grow initially that does not survive the depletion of tubulin as steady state is attained.

That most of the sheared fragments failed to recover, under conditions of net growth, supports one conclusion of Kristofferson *et al.* that the interconversion of a microtubule from unstable (shrinking) to stable (growing) phase is rare (*7*). This contrasts with the results of Horio and Hotani, who observed steady-state microtubules by dark-field microscopy and reported that individual microtubules frequently reversed between growing and shrinking phases (*8*). Under their working conditions, which involved attachment of microtubules to a glass surface, anchorage may have enhanced the stability of a portion of the microtubule core. Kirschner and Mitchison have suggested that anchorage of microtubules to other structures in cells may increase their stability (*2*). The frequency of recovery may also be a function of free tubulin concentration (*11*), which was greater in the dark-field microscopy experiments than in the shearing experiments. Total disassembly of a microtubule after a change to the unstable phase is consistent with observations of microtubules in cells, where the bulk of microtubules depolymerize and are replaced in 10 min (*13*) and where microtubules seem to disappear one at a time (*14*).

Microtubules containing 25% MAPs showed little depolymerization on shearing, indicating the absence of a latent large unstable microtubule core. The minimal depolymerization occurring may be no more than the loss of frayed protofilaments at the fracture points. The survival of multiple fragments from each original microtubule indicates that MAPs act throughout the length of the microtubule, either to stabilize the microtubule lattice or to facilitate immediate recovery back to the growing phase. The limited increase in average microtubule length (from 5 to 6 μm in 30 min) suggests that end-to-end annealing (*12*) contributes little to apparent growth under these experimental conditions.

These experiments supports the concept that microtubules may exist in a metastable state. Although the body of the MAP-depleted microtubule may be inherently unstable, the overall stability of the microtubule is controlled by events at the ends of the polymer. This finding strongly supports the idea that regulation of microtubule assembly in most cells could be determined at sites of microtubule anchorage (*2*). We surmise that MAP-rich microtubules, on the other hand, may be a specialization of brain tissues where stability is more important than dynamics.

REFERENCES AND NOTES

1. T. J. Mitchison and M. W. Kirschner, *Nature* **312**, 232 (1984); *ibid.*, p. 237.
2. M. W. Kirschner and T. J. Mitchison, *Cell* **45**, 329 (1986).
3. F. R. Hallett *et al.*, *Biopolymers* **24**, 947 (1985).

4. F. R. Hallett and R. A. B. Keates, *ibid.*, p. 2403.
5. M. F. Carlier, T. L. Hill, Y. D. Chen, *Proc. Natl. Acad. Sci. U.S.A.* **81**, 771 (1984).
6. Y. D. Chen and T. L. Hill, *ibid.* **82**, 1131 (1985).
7. D. Kristofferson, T. J. Mitchison, M. W. Kirschner, *J. Cell Biol.* **102**, 1007 (1986).
8. T. Horio and H. Hotani, *Nature* **321**, 605 (1986).
9. Microtubule protein, prepared in a mixture of 0.1*M* MES K^+ (the potassium salt of 4-morpholineethanesulfonic acid), 2 m*M* magnesium acetate, and 1 m*M* EGTA buffer, *p*H 6.6 (MME) [R. A. B. Keates, *Can. J. Biochem. Cell Biol.* **62**, 803 (1984)], was estimated to contain 25% MAPs and 74% tubulin by scanning densitometry. We then added NaCl and glycerol to attain concentrations of 0.3*M* and 2*M*, respectively, and the solution was applied to a DEAE-Sepharose CL-6B column (1.5 cm by 8 cm). MAPs were eluted with 0.3*M* NaCl, 2*M* glycerol in MME. MAP-free tubulin was eluted with 0.5*M* NaCl, 2*M* glycerol in MME, and was dialyzed overnight against 5*M* glycerol in MME. We observed that the purified tubulin self-assembled into microtubules after increasing $[Mg^{2+}]$ to 5 m*M*, adding GTP to 1 m*M*, and raising the temperature to 37°C. One cycle of assembly and disassembly after the column step enriched for polymerization-active protein.
10. The sample (prepared and incubated as in Fig. 3A) was illuminated by a HeNe laser (15 mW, 632.8 nm) and was monitored at 90° to the incident beam. Intensity fluctuations detected by a quantum photometer (model 1140, Princeton Applied Research, Princeton, NJ) were correlated with a digital autocorrelator (model 1096, Langley-Ford Instruments, Amherst, MA). The resulting intensity autocorrelation functions were analyzed with a long-rod approximation developed specifically for systems such as microtubules (*3*). We determined microtubule lengths by using the exponential sampling method of Hallett and Keates (*4*), except that a nonnegative least squares routine [I. D. Morrison, E. F. Grabowsky, C. A. Herb, *Langmuir* **1**, 496 (1985)] was included in the fitting procedure. QELS-derived distributions have been verified with microtubule samples measured by electron microscopy (*4*). Typical length distributions were broad and highly skewed; a sample with a mean length of 16 μm contained components from 1 to over 60 μm.
11. R. A. Walker *et al.*, *J. Cell Biol.* **105**, 29a (1987).
12. S. W. Rothwell, W. A. Grasser, H. N. Baker, D. B. Murphy, *ibid.*, p. 863; M. Caplow, J. Shanks, B. P. Brylawski, *J. Biol. Chem.* **261**, 16233 (1986).
13. E. Schulze and M. W. Kirschner, *J. Cell Biol.* **104**, 277 (1987).
14. P. J. Sammak *et al.*, *ibid.*, p. 395.
15. We thank J. Marsh and C. Samuels for technical assistance. This work was supported by grants from the Natural Sciences and Engineering Research Council of Canada.

16 February 1988; accepted 13 July 1988

Accelerated Electron Transfer Between Metal Complexes Mediated by DNA

MICHAEL D. PURUGGANAN, CHALLA V. KUMAR, NICHOLAS J. TURRO,* JACQUELINE K. BARTON*

DNA-mediated long-range electron transfer from photoexcited 1,10-phenanthroline complexes of ruthenium, $Ru(phen)_3^{2+}$, to isostructural complexes of cobalt(III), rhodium(III), and chromium(III) bound along the helical strand. The efficiency of transfer depended upon binding mode and driving force. For a given donor-acceptor pair, surface-bound complexes showed greater rate enhancements than those that were intercalatively bound. Even in rigid glycerol at 253 K, the rates for donor-acceptor pairs bound to DNA remained enhanced. For the series of acceptors, the greatest enhancement in electron-transfer rate was found with chromium, the acceptor of intermediate driving force. The DNA polymer appears to provide an efficient intervening medium to couple donor and acceptor metal complexes for electron transfer.

AN UNDERSTANDING OF HOW ELECtrons are transferred over large distances is essential to the characterization of fundamental redox processes in biology such as oxidative phosphorylation and photosynthesis (*1*). The study of long-range electron transfer also contributes significantly to our ability to construct efficient molecular assemblies that can carry out electrochemical reactions. Studies of electron transfer between excited zinc porphyrins and heme centers in protein-protein complexes and between solvent accessible residues modified with pentammine ruthenium and the interior of structurally characterized metalloproteins have shown that electron transfer can occur over large distances through protein interiors (*2, 3*). Theory indicates that such factors as donor-acceptor distance, thermodynamic driving force, and the nature of the intervening medium are critical in determining rates of electron transfer (*4, 5*). Model compounds with variable exothermicity and distance between donor-acceptor pairs have been synthesized, and the rates of intramolecular electron transfer in these provide benchmarks for studies in more complex polymeric systems (*6, 7*).

We report that the double-stranded DNA polymer may also mediate long-range electron transfer between bound donor-acceptor pairs. The apparent enhancement in photoinduced electron-transfer rates for donor-acceptor pairs bound to DNA versus being free in solution is several orders of magnitude (*8, 9*). This apparent rate enhancement in the presence of DNA could be attributed to (i) the increase in local concentration of bound donor-acceptor pairs, (ii) facilitated diffusion of the bound pair along the DNA helix in a reduced dimensional space, and (iii) long-range electron transfer between donor and acceptor pairs with DNA as the intervening medium. By varying temperature, viscosity, and driving force, we show that DNA-mediated electron transfer from $Ru(phen)_3^{2+}$ to $M(phen)_3^{3+}$, where M = Rh, Cr, or Co, may occur, at least in part, through long-range electron transfer.

A current model for the interaction of tris(phenanthroline) metal complexes with DNA is shown in Fig. 1. The rigid metal complex, $Ru(phen)_3^{2+}$, appears to bind to double-stranded DNA primarily through two distinct modes: (i) intercalation, in which one of the phenanthroline ligands may insert and stack in between the base pairs, and (ii) surface or groove binding, in which the hydrophobicity of the phenanthroline ligands as well as the electrostatic charge of the ruthenium dication stabilize binding against the helical groove of the DNA polyanion (*10, 11*). These binding modes have been characterized primarily through photophysical experiments, such as the differential quenching of two types of ruthenium excited states by anionic quenchers, the retention of polarized emission for the intercalative component when excited with polarized light, and the observation of two distinct lifetimes, 0.6 and 2.0 μs, for the surface-bound and intercalated ruthenium

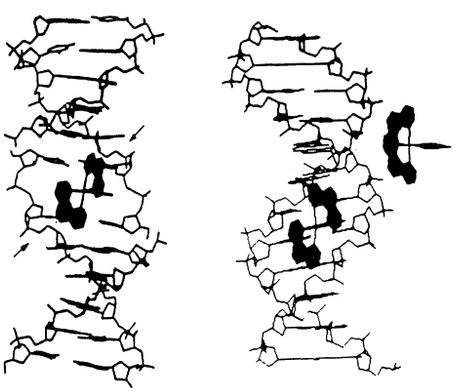

Fig. 1. Model for $Ru(phen)_3^{2+}$ bound to a B-DNA helix, showing (left) intercalation of the Δ-isomer and (right) the surface-binding of the Λ-isomer. For intercalated Δ-$Ru(phen)_3^{2+}$, the intercalated ligand is shown pointed into the page. The arrows indicate the alignment of the non-intercalated ligands along the right-handed helical groove. For the surface-bound Λ isomers, a side view (top) and front view (bottom, with the third ligand pointing out of the page) are shown.

Department of Chemistry, Columbia University, New York, NY 10027.

*To whom correspondence should be addressed.